Analysis and Experimental Validation of SSTDR for Simultaneous Distributed Diagnosis of Wire Networks

Mouad Addad, *Senior Member, IEEE*, Ali Djebbari, *Member, IEEE*, Evan Benoit, and Cynthia M. Furse, *Fellow, IEEE*

***Abstract* — Reflectometry -based techniques such as Spread Spectrum and Sequence Time Domain Reflectometry (S/SSTDR) have been used extensively for the detection, localization, and characterization of electric faults in wires. However, in branched wire networks, testing using a single sensor suffers from ambiguity , where it can be difficult to determine which branch contains the fault. Distributed reflectometry, which uses multiple sensors to test the network from different locations, can resolve this ambiguity. This paper evaluates pseudo -noise (PN) and zero correl ation zone (ZCZ) codes for simultaneous distributed testing . Maximum length (ML or *m*-), Gold and zero correlation zone (ZCZ) codes are compared for a set of up to 16 simultaneous sensors. ML and Gold codes show significant interference between sensors, but the ZCZ codes show near -zero interference over their measurement zone. This lack of interference greatly enhances their use for locating faults. The results were verified numerically and experimentally .**

***Index Terms* —** spread spectrum time domain reflectometry (SSTDR), sequence time domain reflectometry (STDR), distributed reflectometry, non-destructive evaluation, fault location, wire networks, simultaneous testing, continuous diagnosis.

I. Introduction

Wired networks are ubiquitous wherever the transfer of energy and information is needed. They can be found in aircraft, cars, buildings, railways, nuclear power plants, and more. Electrical faults in these systems plague maintainers, driving the need for health monitoring tools able to detect and accurately locate faults. Reflectometry is a powerful technique that has been used extensively for the detection, localization, and characterization of electrical faults [1]. A test signal is injected into the wire, and part of its energy is reflected back to the injection point when it encounters impedance discontinuities within the wire. The test device then extracts information about the location and the nature of these discontinuities from the reflected signal. If the topology of the network is branched, reflections come back from each junction and end of each branch, resulting in multiple, often overlapping, reflections that can lead to ambiguities. If the network has two equal-length arms, one of which has a fault, it is impossible to determine which of the arms is faulty from a single sensor [1- 4]. If an open circuit and a short circuit, which have equal and opposite reflections, are at the same distance from the sensor, their reflections cancel each other out, and neither can be located from a single sensor. Furthermore, the impedance discontinuity between the wire and reflectometer causes an immediate reflection, which results in a "blind zone" in which faults close to the injection point are overshadowed by this reflection. Another challenge for branched networks is that each junction reflects some of the transmitted energy, thus reducing the reflection that returns to the tester. This limits the number of junctions a single tester can see through before the signal is below its detection threshold [4]. Attenuation on long wire lengths exacerbates this problem.

To solve the problems with testing branched networks from a single location, distributed reflectometry uses multiple sensors placed at various points on the wire network [1], [2], [4]. Each sensor provides a different perspective on the network topology. The aggregation of information from all sensors allows the removal of fault location ambiguities and blind zones, and allows testing of longer and more complex networks.

Many algorithms have been used for network evaluation with reflectometry, including multi-channel 1D-CNN [5], iterative calculations [3], [6], twin support vector machines [7], forensic-based investigation algorithm [8], selective averaging [2], wavelet transforms [9], [10], support vector machines [11], residual voltage inversion in cable networks [12], feature-image

This paragraph of the first footnote will contain the date on which you submitted your paper for review.

Mouad Addad is with the Telecommunications and Digital Signal Processing Laboratory, Djillali Liabes University of Sidi Bel Abbes, SBA, Algeria, and a visiting scholar with the Electrical and Computer Engineering Department, University of Utah, Salt Lake City, UT 84112 USA (e-mail: mouad.addad@univ-sba.dz; u6062840@utah.edu).

Ali Djebbari is with the Telecommunications and Digital Signal Processing Laboratory, Djillali Liabes University of Sidi Bel Abbes, SBA, Algeria (e-mail: ali.djebbari@univ-sba.dz).

Evan Benoit is with the Electrical and Computer Engineering Department, University of Utah Asia Campus, Incheon, South Korea (email: evan.benoit@utah.edu)

Cynthia M. Furse is with the Electrical and Computer Engineering Department, University of Utah, Salt Lake City, UT 84112 USA (e-mail: cfurse@ece.utah.edu).

analysis with residual neural networks [13], neural networks [14], residual voltage inversion [15], and time reversal [16].

The algorithms described above require reflection and transmission data, typically from multiple points in the network. This can be accomplished either sequentially or simultaneously. Sequential testing can prevent interference between sensors, but can be time consuming. Also, not all parts of the system are tested at once, and intermittent faults can be missed during this time. For continual testing and monitoring, which we will focus on, each sensor should test continually and simultaneously. For simultaneous testing, signals need to be chosen so that they do not interfere with each other.

Each type of reflectometry uses a different test signal [1]. Time domain reflectometry (TDR) uses a stepped or pulsed incident signal, frequency domain reflectometry (FDR, used in vector network analyzers) uses multiple single-frequency sine waves or a chirp of sine waves of different frequencies, chaos TDR uses injected noise signals, and noise domain reflectometry (NDR) uses existing noise and signals in the system as a passive test system. These techniques are not suitable for testing multiple channels simultaneously, as they would interfere with each other. Testing multiple channels simultaneously requires multiple orthogonal signals. This can be accomplished with spectral time domain reflectometry (STDR) and spread spectrum time domain reflectometry (SSTDR).

In this paper, we focus on enabling simultaneous distributed sensing and diagnosis of branched wire networks using S/SSTDR [17] with zero-correlation zone codes (ZCZ). The advantage of these sequences is that they do not interfere with each other over a specific zone, which can greatly improve testing accuracy. This has been previously introduced in [18], [19], [20]. In this paper, we validate these results with measurements and simulations on a Y-shaped branched network. We compare *m*-, Gold, and ZCZ sequences to determine how much interference will be seen with up to 16 sensors working simultaneously (which gives 15 interferers for each sensor).

This paper is organized as follows. Section II describes the analytical model of the distributed diagnostic system. Section III discusses the selection of suitable signals that provide interference-free measurements. Section IV describes experimental validation, and Section V describes verification with simulation. The discussion and conclusion in Section VI describe how to adapt these results to other systems.

II. System Model

A block diagram of and S/SSTDR system for testing a wire network from multiple locations (distributed sensing) is shown in Fig. 1.

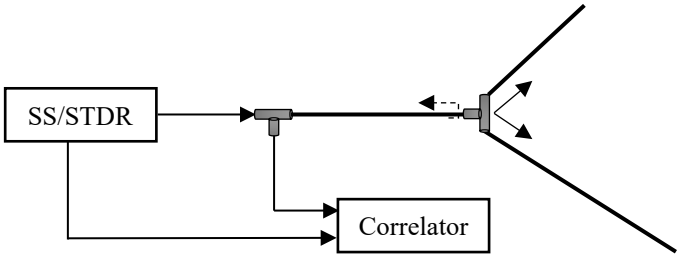

Fig. 1. Block diagram of an SS/STDR system.

An STDR test signal consists of a square wave modulated by a sequence as in

$$s_i(t) = \sum_{n=-\infty}^{\infty} s_{i,n}\, p(t - nT_c) \tag{1}$$

where sequence $s_{i,n} \in \{-1,1\}$ has a chip width, T_c, and the rectangular pulse waveform $p(t)$ is defined as

$$p(t) = \begin{cases} 1 & 0 \le t \le T_c \\ 0 & \text{otherwise} \end{cases} \tag{2}$$

Note that $s_i(t)$ is a periodic signal with period $T = NT_c$, where N is the sequence length, so that $s_i(t) = s_i(t + T)$. After transmission onto the wire network, the received signal at the i^{th} sensor is

$$r(t) = a_o s_i(t) + \sum_{p} a_p s_i(t - \tau_p) + \sum_{\substack{k=1 \\ k \neq i}}^{K} b_k s_k(t - \tau_k) + d(t) + n(t) \tag{3}$$

where a_o is the amplitude of the reflection at the testing point due to the impedance mismatch between the measurement device and the wire. a_p and τ_p are, respectively, the attenuation coefficients and delays of the test signal $s_i(t)$ reflecting from an unknown number p of impedance mismatches in the network, $d(t)$ is the data signal on the network, b_k and τ_k are, respectively, the attenuation coefficients and delays of a different test signal, $s_k(t)$, coming from the k^{th} sensor, and $n(t)$ is the noise signal.

The reflected signal carries information about the status of the wire network, and many algorithms are available to extract the network topology, detect and locate faults, etc. [1]. Interference caused by the signals from all sensors working simultaneously, data signals, and noise can perturb the received signals. The effects of noise can be reduced through averaging [18] and other de-noising techniques. In this paper, we will focus on choice of sequences to reduce interference from multiple sensors transmitting and receiving simultaneously. For STDR, the received signal $r(t + \tau)$ is cross correlated with a reference signal $s_i'(t)$, typically the incident signal. Signals testing continuously are periodic, so the periodic cross correlation function is used:

$$R_{rs_i'}(\tau) = \frac{1}{T}\int_0^T s_i'(t)\, r(t + \tau)\, dt \tag{4}$$

The delay τ is proportional to the distance $2d$ over which the signal travels

$$2\,d = v\,\tau \tag{5}$$

where v is the velocity of propagation (*VOP*) on the wire, and the factor of *2* comes from travel to and from the fault.

The magnitude of the correlation in (4) depends on the length of the signals and how well correlated they are, as we will show in Fig. 2. By substituting (3) in (4), we obtain the correlation of the complete received signal

$$R_{rs_i'}(\tau) = a_o R_{s_i s_i'}(\tau) + \sum_p a_p\, R_{s_i s_i'}(\tau - \tau_p) + \sum_{\substack{k=1 \\ k\neq i}}^{K} b_k\, R_{s_k s_i'}(\tau - \tau_k) + R_{ns_i'}(\tau) \tag{6}$$

The first term is self-correlation of the incident signal of interest, and the second term is correlation of its reflections. Both of these signals are desired for evaluation of the network. The third term is interference from other sensors simultaneously testing on the same network, and the fourth term is correlation with the noise and other signals on the line. The last two terms are not desirable, and we should minimize them by choosing signals with low cross-correlation. Equation (6) shows that the correlator's output depends on the correlation properties of the incident sequence. To further clarify this point, let's rewrite the first term of (6) as follows

$$R_{s_i s_i'}(\tau) = \sum_{m=0}^{N-1}\sum_{n=0}^{N-1} s_{i,m} s_{i,n} \frac{1}{T}\int_0^T p(t - mT_c)p(t + \tau - nT_c)\,dt \tag{7}$$

The integral in (7) is nonzero only when $p(t - mT_c)$ and $p(t + \tau - nT_c)$ overlap. The delay $\tau = lT_c + \tau_\phi$, where $0 \le \tau_\phi < T_c$ is any delay, not necessarily an integer number of chips. Using this substitution, the pulses overlap only for $n = m + l$ and $n = m + l + 1$, so that (7) becomes

$$R_{s_i s_i'}(\tau) = \left(1 - \frac{\tau_\phi}{T_c}\right) E_{s_i s_i'}(l) + \frac{\tau_\phi}{T_c} E_{s_i s_i'}(l+1) \tag{8}$$

The discrete periodic cross correlation function (PCCF) of two sequences s_k and s_i' is defined as

$$E_{s_k s_i'}(l) = \frac{1}{N}\sum_{n=0}^{N-1} s_{k,n} s'_{i,n+l} \tag{9}$$

where the subscript $n + l \ge N$ is computed modulo N. When $k = i$, the PCCF becomes the periodic autocorrelation function (PACF). Similarly, it can also be shown that the autocorrelation of one of the reflections in (6) with a delay τ_p from the wire network is

$$R_{s_i s_i'}(\tau - \tau_p) = \left(1 - \frac{\tau_\phi}{T_c}\right) E_{s_i s_i'}(l - l_p) + \frac{\tau_\phi}{T_c} E_{s_i s_i'}(l - l_p + 1) \tag{10}$$

and a similar cross correlation between reference and an interference signal in (6) is

$$R_{s_k s_i'}(\tau - \tau_k) = \left(1 - \frac{\tau_\phi}{T_c}\right) E_{s_k s_i'}(l - l_k) + \frac{\tau_\phi}{T_c} E_{s_k s_i'}(l - l_k + 1) \tag{11}$$

Note that in the special case where reference and reflection signals are shifted by an integral number of chips, $\tau = lT_c$, Equation (6) becomes

$$R_{rs_i'}(\tau) = a_o E_{s_i s_i'}(l) + \sum_p a_p\, E_{s_i s_i'}(l - l_p) + \sum_{\substack{k=1 \\ k\neq i}}^{K} b_k\, E_{s_k s_i'}(l - l_k) + R_{ns_i'}(\tau) \tag{12}$$

A similar expression was obtained in [18] where $R_{rs_i'}(\tau)$ is dependent on the *aperiodic* correlation properties. In contrast, (12) depends on the *periodic* correlation properties. Also, similar results can be obtained for spread spectrum time domain reflectometry (SSTDR), which uses a sine wave (or other function) modulated by the STDR signal. The performance of the diagnostic system is improved if sequences with low cross correlation and high autocorrelation are used.

III. SELECTION OF SEQUENCES

According to (12), the nonzero side-lobes of the PACF cause interference of the test signal with itself (self-interference) and the nonzero PCCF causes interference between test signals generated by other sensors in the network (mutual interference). Therefore, the optimal sequence set should have impulse-like PACF (zero side lobes) and zero PCCF. Among the conventional sequences, maximal-length *m*-sequences have the smallest PACF side lobes (-1). The disadvantage of these sequences is their PCCF peaks which increase rapidly with sequence length. Consequently, *m*-sequences are optimal for single-point diagnostic systems, but not for simultaneous distributed sensing. Large sets of sequences with relatively good PCCF such as Gold sequences can be generated from a pair of *m*-sequences called the preferred pair. Zero Correlation Zone (ZCZ) sequences have recently been introduced to the field of wire diagnostics. Their performance was evaluated in the case of simultaneous diagnosis of multiple wires in [19], distributed diagnosis of noisy wire networks in [18], and simultaneous diagnosis of shielded cable bundles in [20]. The distinctive property of ZCZ sequences is that they have a zero-correlation zone in both their PACF and PCCF, where they are ideal for testing. If the zero-correlation zone width is chosen to be large enough to encompass all of the significant reflections in the system, interference from other codes transmitting simultaneously can be eliminated. To do this, the zero-correlation zone Z_o must satisfy the following bound:

$$Z_o \ge \frac{2\,d}{v\,T_c} \tag{13}$$

where $2d$ is the distance the farthest reflection will travel in the wired network, v is the *VOP* in the wire, T_c is the chip duration.

For example, if the chip rate is $R_c = 25\,MHz$ then the corresponding chip duration is $T_c = 1/R_c = 40\,ns$. By assuming the propagation speed in wires to be two-thirds the speed of light $v = 2\,x\,10^8\,m/s$ and the zero zone equal to 16 chips, the interference can be reduced up to a distance equal

to $d = 64\,m$ from the testing point. The periodic correlation properties of 16 ZCZ sequences each of length $N = 512$ are shown in Fig. 2. The $d = 64m$ zone is seen (after which, the desired zero correlation disappears). A performance metric based on the merit factor was proposed in [19] to evaluate the effectiveness of different sequences. This metric is a ratio of the autocorrelation peak (representing the desired signal) and the cross-correlation sidelobes (representing the interference). It was shown in [18] that ZCZ sequences are promising candidates for simultaneous and distributed diagnosis due to their favorable correlation properties.

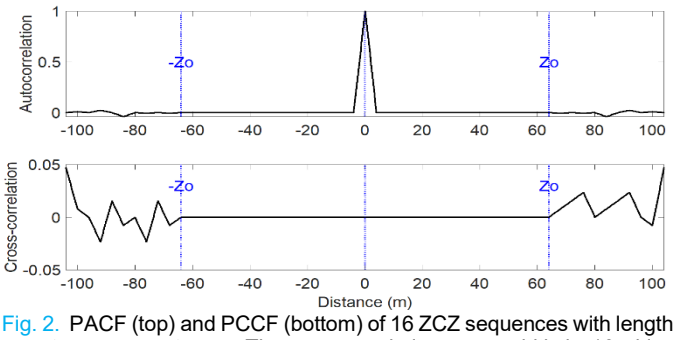

Fig. 2. PACF (top) and PCCF (bottom) of 16 ZCZ sequences with length $N = 512$, $Rc = 25\,MHz$. The zero-correlation zone width is 16 chips (corresponding to 64 m) long.

ZCZ sequences are significant because they eliminate the noise term in (12), giving:

$$R_{rs_l'}(\tau) = a_o\delta_l + \sum_p a_p\,\delta_{l-p} \qquad (14)$$

where δ_l is the Kronecker delta function defined as

$$\delta_l = \begin{cases} 0 & \text{if } l \neq 0 \\ 1 & \text{if } l = 0 \end{cases} \qquad (15)$$

In this case, both self-interference and mutual interference are eliminated. The drawback of these sequences is the tradeoff between the zero-correlation zone width and the number of sequences available for a specific sequence length. For more details, refer to Table 1 in [19]. Consequently, ZCZ sequences are more suitable for distributed diagnostic systems where the number and location of sensors are judiciously chosen.

IV. Experimental Validation

To validate the effectiveness of properly chosen ZCZ sequences for distributed sensing, we measure reflection from a simple Y-shaped wire network with a single sensor and sequence. We then add up to 15 simultaneous sequences as interferers. We compare *m*-, Gold, and ZCZ sequences.

1) Test Setup

We use a Rohde & Schwarz MXO5 oscilloscope with two waveform generators, used as shown in Fig. 3.

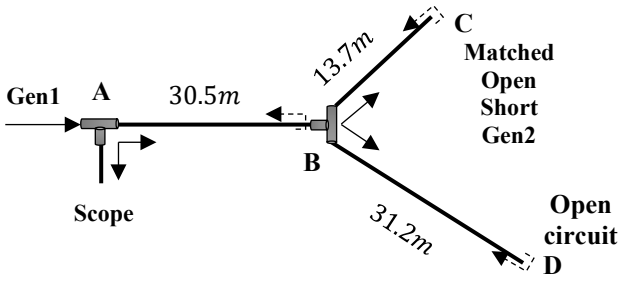

Fig. 3. Experimental setup for simultaneous diagnosis using SS/STDR distributed reflectometry.

The function generators in the scope output predefined waveforms at 625 Msample/s, while its arbitrary waveform generators output user-defined waveforms with rates up to 312.5 Msample/s. We generated a signal sequence using MATLAB and uploaded it to the arbitrary waveform generator. The signal was captured by using one of the input channels (8 channels) with input impedance that can be set to either 50 Ω or 1 MΩ. An example of 30 chips of a 25 MHz m-sequence signal is shown in Fig. 4. The theoretical and measured values (using a direct connection between generator and scope) are compared.

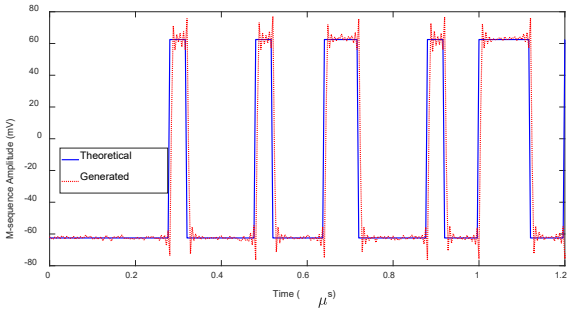

Fig 4. First 30 chips of the 25 MHz m-sequence comparing the ideal (theoretical) and measured (generated) time domain values.

Three RG-58 coaxial cables with characteristic impedance 50Ω are used to form the Y-network. Generator 1 (Gen1) is connected at A to a 30.5 m cable, which connects at B to a T-junction of 13.7 m and 31.2 m cables. The BNC T-adapter at A also connects channel 1 of the oscilloscope. The signals are generated based on sequences uploaded from MATLAB™. These are either STDR or SSTDR. The STDR is a square wave modulated by a sequence (as in (1), shown in Fig. 4), and the SSTDR is a sine wave modulated by the STDR signal. The sequences are of length $N = 511$ for *m*- and Gold sequences, and $N = 512$ for ZCZ sequences. The chip rate is $25\,MHz$, giving a chip duration of $T_c = 40\,ns$. The sequence is up-sampled by a factor of $N_s = 10$, so the sample rate is $250\,MHz$. The highest sampling rate available for this generator is slightly above $300\,MHz$. The reflected signals come back to the scope through the T-junction at A. Then the signals are downloaded and processed (cross-correlated with the incident signal) using MATLAB™.

2) Single-Point Diagnosis of Wire Network

In this section, we consider reflection from the wired network in Fig. 3 using only Gen 1 at A, transmitting an *m*-sequence. We expect *m*-sequences to be optimal for single-point diagnostic systems. The $25\,MHz$ STDR *m*-sequence has a length $N = 511$ and is up-sampled to $250\,MHz$. The distance

from Gen1 is calculated as *d=v/(2 x time)*, where v=2 $x10^8$ m/s is 2/3 the speed of light. The factor of two in the denominator comes from the wave traveling to the end of the cable and back. The signal amplitude is 62.5 mV. This was chosen, so that the sum of this signal plus (in later sections) 15 additional sequences representing additional distributed sensor units (and consequent interferers) would remain under the maximum allowable voltage of the function generator (5 V_{peak}). Increasing the amplitude of the test signal will raise the correlation peak amplitudes, however, the overall shape of the response remains unchanged. The test signal is a square wave modulated by a sequence, with each chip having a duration of $T_c = 40\,ns$, which corresponds to sampling distance of 8 m. The sequence is up-sampled by a factor of $N_s = 10$ resulting in a sample width of 4 ns corresponding to a sampling distance of 0.8 m. If we increased T_c, this would decrease the bandwidth of the signal, increase correlation pulse width, and decrease the overall accuracy of the test.

The diagnosis of the wired network can be in either continuous mode, where the periodic STDR signal transmits continuously and is correlated continuously, or in non-continuous mode, where only one period of the *m*-sequence is used. A detailed analysis can be found in [18]. The correlated reflection signatures of the wire network in Fig. 3 to the two diagnostic modes are plotted in Fig. 5.

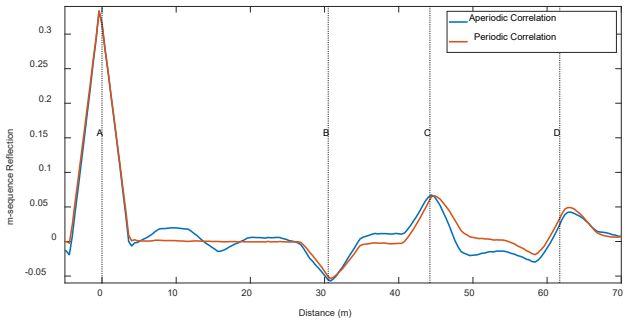

Fig. 5. STDR response from a Y-shaped network using non-continuous (aperiodic) and continuous (periodic) monitoring with an *m*-sequence. Locations ABCD are shown in Fig. 3.

The peaks in Fig. 5 are from impedance discontinuities in the network. The first peak (A) corresponds to the T-junction connecting Gen1 and the scope to the first cable. The magnitude of a reflection at a T-junction between cables of equal impedance is 1/3, so we have used this value to normalize the correlation, giving the reflection amplitudes shown in Fig. 5 and others. The second peak is from the junction at B. Peak C (at 44.2 m) is from the end of the 13.7 m cable. Peak D (at 61.7m) is from the end of the 31.2 m cable. The response using periodic correlation is smoother than the one using aperiodic correlation, which is due to the continuous nature of the diagnostic system. When the periodic correlation is performed, only the even PACF (12) is computed. For a non-continuous diagnostic system, another type of correlation function called the odd periodic correlation function (OPACF) must also be considered. The effect of the OPACF can be seen in the fluctuation of the response using aperiodic correlation.

A. View from Generator 1

The periodic correlated reflection response of the Y-shaped network in Fig. 3 using a single generator (Gen1 at A) is shown in Fig. 6. The generator is matched (50Ω), the end of 31.2m cable is an open circuit, and the end of the 13.7 cable is either matched (50 Ω), open, or short. Gen1 injects STDR *m*-, Gold, or ZCZ sequences. The test signal of amplitude is 62.5 mV is injected continuously, forming a periodic signal. The combination of incident and periodic reflection signals is collected by the scope. This is correlated with the incident signal offline, which is obtained by connecting Gen1 directly to the scope. The correlated signals are shown in Fig. 6. All sequence types perform well in this case with no interference. The *m*-sequence is the best, as expected. The peak at A, seen in Fig. 6 at $x = 0$, is caused by the reflection at the first T-junction. The second peak (B) is from the second T-junction used to form the Y-network at 30.5 m. Peak C from the end of the 13.7m cable appears at 44.2 m, the combination of the 30.5m and 13.7m cables. The positive peak at C is from the open, the negative from the short, and the lack of peak from the matched load. Finally, peak D from the open end of the 31.2m cable appears at 61.7 m. Additional smaller reflections (not shown) follow from multiple reflections within the network. A similar correlated reflection response from SSTDR is shown in Fig. 7.

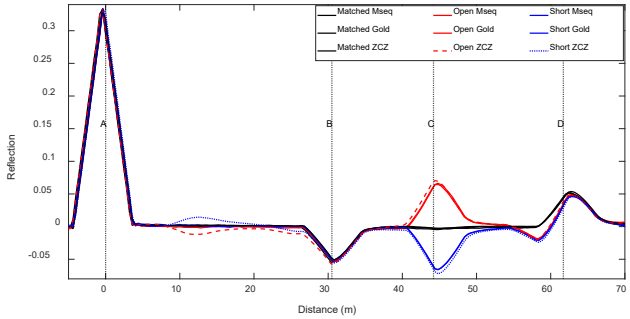

Fig. 6. STDR response of the Y-shaped network in Fig. 3 using *m*-, Gold, or ZCZ sequences applied at Gen1 at A. The end of the 13.7m cable is matched, open, or short. Gen2 is not active.

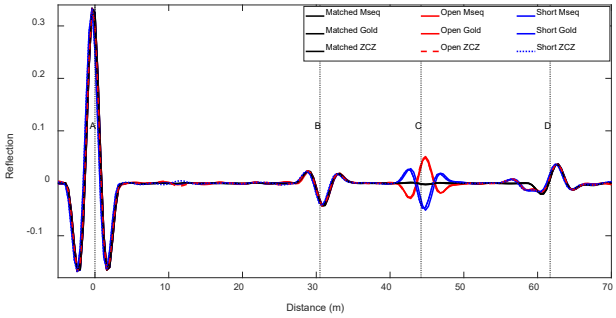

Fig. 7. SSTDR response of the Y-shaped wire network in Fig. 3 using *m*-, Gold, or ZCZ sequences at Gen1. The end of the 13.7m cable is matched, open, or short. Gen2 is not active.

B. View from Generator 2

In Section A, from the point of view of only Gen1 at A, we cannot determine which peak (at 30.5 m and 61.7m) corresponds to the end of which cable branch. To remove this ambiguity, another sensor (Gen 2 at C) is used. For the network in Fig. 3, Gen1 at A is replaced by either an open, short, or matched load, and the injected signal is from Gen2 at C

(connected to the scope through a T-junction). The correlated reflection is shown in Fig. 8.

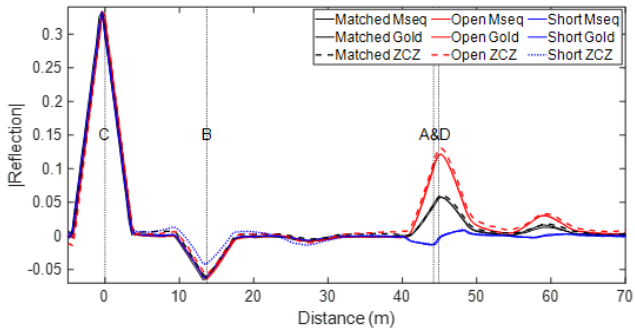

Fig. 8. STDR response of the Y-shaped network in Fig. 3 using Gen2 to apply *m*-, Gold, or ZCZ sequences at C, where the scope is connected. The cable at A is matched, open, or short.

As in Fig. 6, the peak at C (*x=0)* is caused by the T-junction between Gen2, the scope, and the 13.7 m cable. The peak at B is from the T-junction between all three cables. At AD (44.2 m), we see a peak corresponding to reflections that add up from open circuits at A and D.

3) Distributed Diagnosis of Wire Network

We now evaluate a simultaneous and distributed diagnosis of the network. Gen1 at A sends one STDR signal while Gen2 at C sends additional signals to simulate multiple distributed sensors on other parts of the network. With all sensors working simultaneously, signals from Gen2 cause some interference with those from Gen 1, which we evaluate in this section.

A. *View from Generator 1*

The correlated reflection signatures measured at Gen1 (originally seen in Fig. 6) are shown in Fig. 9.

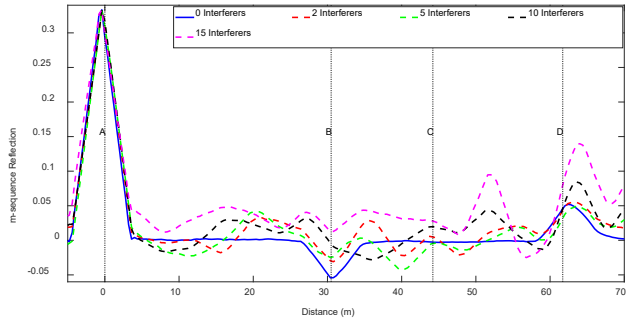

(a)

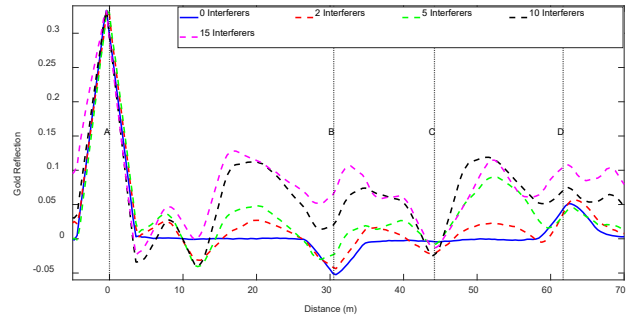

(b)

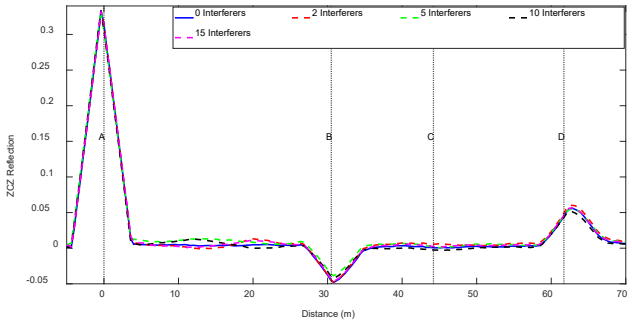

(c)

Fig. 9. STDR response of the Y-shaped wire network in Fig. 3 using Gen1 (at A). Gen2 (at C) is matched. Gen2 injects up to 15 interference signals that are (a) *m*-, (b) Gold, or (c) ZCZ sequences.

Additional signals (interferers) are sent into the system by Gen2. Up to 15 additional signals (each with amplitude 62.5 mV) are added up, slightly delayed from each other, and sent into the system by Gen2 at C. Significant measurement interference is seen for *m*- and Gold sequences, but little interference is seen for ZCZ sequences. It is important to note that the amplitude of the signals was chosen so that when constructive interference (the sum) of all 15 sequences occurs, which will give 15 times the original amplitude, the function generator would not clip this total amplitude. Also, the reason sequences were added up out of sync by portions of a chip is that there is more interference from this than from sequences that are delayed by an integer number of chips. The interference signals have a significant impact on the diagnostic capability of the system, as shown in Fig. 9. Even two interferers are enough to cause ambiguity when *m*- and Gold sequences are used. ZCZ sequences, with their ideal correlation properties, are not impacted by other interferers in this time/distance zone. The normalized interference error, obtained from Fig. 9, is defined as the average difference between measurements with 0 and 15 interferers across the zero-correlation zone range 0–64 m, normalized by the magnitude of the peak response at point A. For *m*-, Gold, and ZCZ sequences, the normalized interference error values are 0.125, 0.2, and 0.006, respectively. Similar trends are observed for SSTDR measurements in Fig. 10, where *m*- and Gold sequences exhibit normalized interference errors of 0.051 and 0.08, respectively, while ZCZ sequences show a significantly lower error of 0.003.

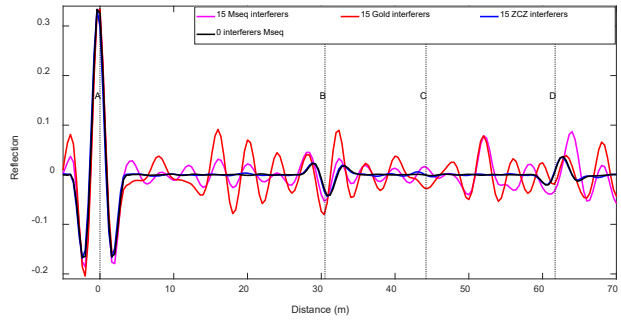

Fig. 10. SSTDR response of the Y-shaped wire network in Fig. 3 is applied at Gen1(at A). Gen2 (at C) is matched and injects 15 interference signals that are *m*-, Gold, or ZCZ sequences.

B. *View from Generator 2*

We now switch our view of the network from A to C. Gen2 (C) injects an STDR signal, and Gen1 (A) injects 5 interference

signals. The reflection response is shown in Fig. 11.

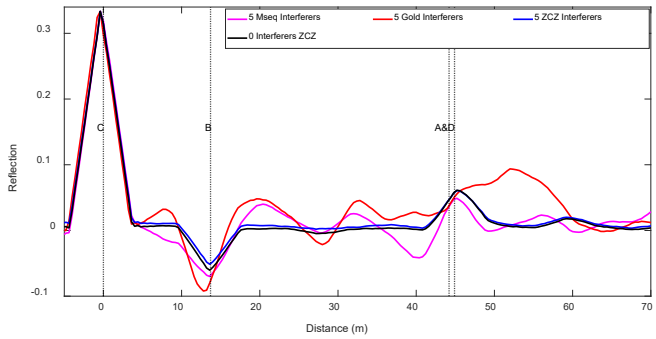

Fig. 11. STDR response of the Y-shaped network in Fig. 3. The signal is applied at Gen2 (at C). Gen1 (at A) is matched and injects 5 interference signals that are *m*-, Gold, or ZCZ sequences.

V. Simulation Results

The results in section IV demonstrate the relative interference of *m*-, Gold, and ZCZ sequences for distributed sensing. The specific examples were done at 25 MHz, where the 16 ZCZ sequences 512 chips long have a zero-correlation zone of 64 m. We would like to be able to extend these results to other applications, with different frequencies, sampling rates, sequence lengths, zero correlation zones, numbers of interferers, etc. For this purpose, we have developed a simulation tool. A bounce diagram is used to determine the expected magnitudes and time delays of reflections and transmissions within the wire network. These magnitudes and time delays are used to determine an expected correlation signature for each reflection, and then all reflections are added to create the total correlation signature. For the wire network in Fig. 3 with Gen 1 transmitting a single sequence at A and Gen 2 transmitting 15 interfering signals at C, the correlated reflection response is shown in Fig. 12 for *m*-, Gold, and ZCZ sequences. This is comparable to the measured data shown in Fig. 6 with C an open circuit or high impedance generator. The various levels of interference for the different sequence types are comparable to Fig. 9 with 15 interferers.

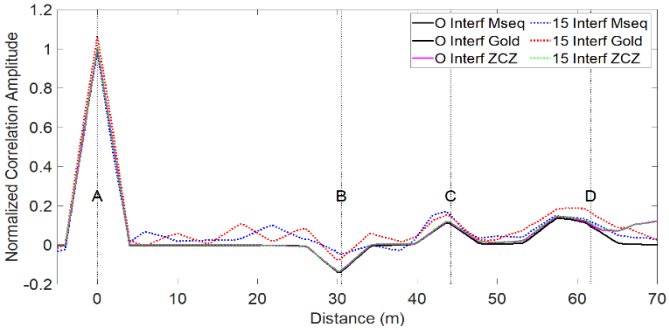

Fig. 12. Diagnosis of Y-shaped wire network using STDR using *m*-, Gold, or ZCZ sequences. Gen. 1 (at A) is testing, and Gen. 2 (at C) injects 15 interference signals.

VI. Discussion and Conclusion

This paper concentrates on enabling distributed sensing and diagnosis of branched wire networks using spread spectrum and sequence time domain reflectometry (S/SSTDR) with zero-correlation sequences (ZCZ). The advantage of these sequences is that they have literally zero correlation over a specific zone (in time or space), which can greatly improve testing accuracy. This has been previously introduced in [18], [19], [20]. In this paper, we validated these results with measurements on a Y-shaped branched network. We compared *m*-, Gold, and ZCZ sequences to determine how much interference will be seen from one test sequence with up to 15 interferers. As expected, we saw that *m*-sequences are very effective (have low self-interference) when only one sequence is used. This would be ideal for testing from a single point, with no additional interference present in the system. However, in distributed sensing, where testing is done from multiple locations to improve the diagnostic options for the system, the interference from simultaneous testing is substantial and problematic for both *m*- and Gold sequences. The ZCZ sequences show near-perfect zero correlation over their expected zones, thus enabling much better test results. Outside of their zone, the interference is significant, so these sequences should be carefully designed for each application (frequency, zone length, and desired number of available sequences) to ensure ideal testing. The zone length (Z_o), sequence length (N chips), and number of available ZCZ sequences (M) are related as

$$Z_o = \frac{N}{M} - 1 \tag{16}$$

In addition to validating the performance of the ZCZ sequences on a simple Y-network, a numerical simulation was developed to allow us to consider more complex networks and different sequence parameters for other applications. To work on smaller length systems, we can increase the frequency and decrease the zero-correlation zone time $Z_o(s)$. The zone length in seconds is $Z_o(s) = Z_o Tc$, and in meters is $Z_o(m) = Z_o(s)\,VOP$. This means that the zero-correlation zone, in seconds or meters, scales inversely with frequency. For example, if we scale the 25 MHz ZCZ sequence set—with 16 sequences that are 512 chips long, as used in the sections above—to the same set of sequences at 4 GHz, the zone in meters is $Z_o(m) = 0.8\,m$. This is an appropriate size for many types of imaging systems, such as microwave-based breast cancer detection. For larger systems, or those with many resonances or multiple reflections, a longer $Z_o$may be needed. In that case, longer sequences (larger N) should be used, or fewer sequences (smaller M) will be available. The VOP , which can be impacted by wire and system parameters, also impacts these results, In the case of a wired network, this is relatively minimal, because the vast majority of wires have a VOP that is approximately (within 10%) of 2/3 the speed of light. Attenuation doesn't impact these results with respect to the ZCZ codes, but it does reduce the magnitude of responses from later time/distance.

These results demonstrate and validate the effectiveness of using ZCZ sequences for distributed testing with multiple STDR or SSTDR sensors operating simultaneously to assess a system from multiple vantage points.

Disclosure

Dr. C. M. Furse is a co-founder of LiveWire Innovation, Inc. that is commercializing SSTDR technology, and therefore she is disclosing a financial conflict of interest.

ACKNOWLEDGMENT

The authors gratefully acknowledge financial support for this research by the Fulbright Visiting Scholar Program, which is sponsored by the U.S. Department of State. Its contents are solely the responsibility of the author and do not necessarily represent the official views of the Fulbright Program or the Government of the United States. The authors would also like to thank Rhode-Schwarz for loaning the MXO5 oscilloscope.

REFERENCES

[1] C. M. Furse, M. Kafal, R. Razzaghi, and Y.-J. Shin, "Fault Diagnosis for Electrical Systems and Power Networks: A Review," *IEEE Sensors J.*, vol. 21, no. 2, 2020.

[2] A. Lelong, L. Sommervogel, N. Ravot, and M. O. Carrion, "Distributed reflectometry method for wire fault location using selective average," *IEEE Sensors J.*, vol. 10, no. 2, pp. 300–310, 2009.

[3] C. Lo and C. Furse, "Modeling and simulation of branched wiring networks," *ACES J.*, vol. 23, no. 2, p. 143, 2008.

[4] F. Auzanneau, N. Ravot, and L. Incarbone, "Chaos time domain reflectometry for online defect detection in noisy wired networks," *IEEE Sensors J.*, vol. 16, no. 22, pp. 8027–8034, 2016.

[5] Q. Huang, Z. Li, Z. Fu, Y. Hu, Q. Fang, and Y. Wei, "Complex Wired Network Fault Diagnosis Based on Distributed Reflectometry and Multi-Channel 1D-CNN," *IEEE Sensors J.*, vol. 25, no. 11, pp. 19415–19427, Jun. 2025, doi: 10.1109/JSEN.2025.3559086.

[6] C. Lo, K. Nagoti, A. W. Mahoney, Y. Chung, and C. Furse, "Detection and Mapping of Branched Wiring Networks from Reflectometry Responses," Joint FAA/DoD/NASA Conf. on Aging Aircraft, Palm Springs, CA, Feb. 2005.

[7] A. Goudjil and M. K. Smail, "Wiring Network Diagnosis Using Reflectometry and Twin Support Vector Machines," *Sustainability*, vol. 17, no. 5, Art. no. 5, 2025

[8] Z. Lacheheb *et al.*, "Topology reconstruction of wiring networks using an iterative process based on Time-Domain Reflectometry and Forensic-Based Investigation algorithm," *Nondestructive Testing and Evaluation*, pp. 1–33, 2025.

[9] S. J. Chang and J. B. Park, "Multiple Chirp Reflectometry for Determination of Fault Direction and Localization in Live Branched Network Cables," *IEEE Trans. Instrum. Meas.*, vol. 66, no. 10, pp. 2606–2614, 2017

[10] C.-K. Lee and S. J. Chang, "A Method of Fault Localization Within the Blind Spot Using the Hybridization Between TDR and Wavelet Transform," *IEEE Sensors J.*, vol. 21, no. 4, pp. 5102–5110, 2021

[11] X. Zhang, M. Zhang, and D. Liu, "Reconstruction of faulty cable network using time-domain reflectometry," *Progress In Electromagnetics Research*, vol. 136, pp. 457–478, 2013.

[12] C. Chen, Q. Guan, Q. Guan, X. Jin, and Z. Shi, "Soft Fault Location and Imaging Using Residual Voltage Inversion in Cable Networks," *IEEE Trans. Instrum. Meas.*, vol. 74, pp. 1–16, 2025

[13] D. Liang *et al.*, "Advanced Sensing Techniques for Cable Fault Detection Enhanced by Power-Line Communications and Integrated Feature-Image Analysis with Residual Neural Networks," *IEEE Sensors J.*, 2025.

[14] M. K. Smail, T. Hacib, L. Pichon, and F. Loete, "Detection and Location of Defects in Wiring Networks Using Time-Domain Reflectometry and Neural Networks," *IEEE Trans. Magnetics*, vol. 47, no. 5, pp. 1502–1505, 2011

[15] C. Chen, Q. Guan, Q. Guan, X. Jin, and Z. Shi, "Soft Fault Location and Imaging Using Residual Voltage Inversion in Cable Networks," *IEEE Trans. Instr. Meas.*, vol. 74, pp. 1–16, 2025,

[16] M. Kafal, N. Grégis, J. Benoit, and N. Ravot, "An Effective Method Based on Time Reversal and Optimization Techniques for Locating Faults on Power Grids," *IEEE Sensors J.*, vol. 21, no. 2, pp. 1092–1099, 2021

[17] S. Kingston *et al.*, "A SSTDR methodology, implementations, and challenges," *Sensors*, vol. 21, no. 16, p. 5268, 2021.

[18] M. Addad and A. Djebbari, "Spread Spectrum Sensing Based on ZCZ Sequences for the Diagnosis of Noisy Wired Networks," *IEEE Sensors J.*, vol. 21, no. 2, pp. 914–920, 2020.

[19] M. Addad and A. Djebbari, "Simultaneous multiple cable fault locating using zero correlation zone codes," *IEEE Sensors J.,* vol. 21, no. 2, pp. 907–913, 2020.

[20] M. Addad and A. Djebbari, "Spread spectrum reflectometry for the simultaneous diagnosis of shielded cable bundles," *Nondestructive Testing Eval.*, vol. 39, no. 4, pp. 939–953, 2024.

Mouad Addad (M'22-SM'25) received his Ph.D. degree in Telecommunications from Djillali Liabes University of Sidi Bel Abbes, Algeria, in 2018. He joined the Telecommunications Department at the same University in 2018, where he is currently an Associate Professor. From 2017 to 2018, he was a visiting Ph.D. student at IEMN institute in Valenciennes, France. In September 2024, he joined the Electrical and Computer Engineering Department at the University of Utah as a Visiting Scholar.

Ali Djebbari (M'25) received his Ph.D. degree in Signal Processing from the University of Sciences and Technology of Oran (USTO), Algeria, in 1997. In 1991, he joined the Djillali Liabes University as an Assistant Professor, became a Lecturer in 1997, and was promoted to Full Professor in 2003. He was promoted to Distinguished Professor in 2025. Since 2000, he has been the Director of the Telecommunications and Digital Signal Processing Laboratory. He is currently with the Telecommunications Department at Djillali Liabes University.

Evan Benoit received his Ph.D. in Electrical Engineering from the University of Utah in 2023. His research was in electromagnetics and transmission line theory, specifically, in the use of Time Domain Reflectometry to measure impedance. He then joined the Electrical and Computer Engineering department at the University of Utah Asia Campus in Incheon, South Korea as an Assistant Professor (Lecturer) where he currently teaches Physics I and II, as well as undergraduate ECE courses.

Cynthia M. Furse (M'85–SM'99–F'08) is a Distinguished Professor of Electrical and Computer Engineering at the University of Utah. She applies electromagnetics to sensing and communication in complex lossy media such as the human body. She is a Fellow of the IEEE, the National Academy of Inventors, and the Applied Computational Electromagnetics Society and has received numerous teaching and research awards including the 2020 IEEE Chen To Tai Distinguished Educator Award and the 2025 Harrington-Mittra Award in Computational Electromagnetics.